Sensors and Actuators A 161 (2010) 66–71

Contents lists available at ScienceDirect

Sensors and Actuators A: Physical

journal homepage: www.elsevier.com/locate/sna

Sensing micrometer-scale deformations via stretching of a photonic crystal

N.L. Privorotskaya [a], C.J. Choi [b], B.T. Cunningham [b], W.P. King [a,*]

[a] Department of Mechanical Science and Engineering, University of Illinois Urbana-Champaign, United States
[b] Department of Electrical and Computer Engineering, University of Illinois Urbana-Champaign,United States United States

ARTICLE INFO

Article history:
Received 3 December 2009
Received in revised form 15 May 2010
Accepted 17 May 2010
Available online 1 June 2010

Keywords:
Strain sensor
Microstrain
Photonic crystal

ABSTRACT

This paper reports micrometer-scale strain measurements that are enabled through the observed wavelength shift in a stretched surface photonic crystal narrow bandwidth optical reflectance filter. The photonic crystal optical filter is comprised of a 550 nm period, dielectric-coated linear grating structure, which was fabricated on the surface of a thin sheet of silicone rubber. When stretched, the change in grating period induced a change in the wavelength of light coupled into the photonic crystal, which could be measured using a spectrometer. The observed wavelength change was 4.53 nm per 1% strain and was linear up to 3.75% strain. The measurement was affected by temperature fluctuations, which could be compensated. The resolution of the measurement was 78 $\mu\varepsilon$.

1. Introduction

Considerable research effort has concentrated on using mechanically deformable optical structures, including passive resonators such as three-dimensional photonic crystals for optical modulation [1–5]. Previous work has demonstrated that simple one-dimensional and two-dimensional surface photonic crystals (PCs) (also known in the literature as guided-mode resonant filters) are capable of performing as narrowband reflectance filters, in which the PC period, and refractive indices of the structural materials can be manipulated to design structures that selectively couple to a desired wavelength spanning the ultraviolet to infrared [1,2,6,7]. The PC approach essentially relies on the coupling of light that is trapped within the high index device layers as resonant modes to free-space via the creation of leaky modes by periodic structuring [3,4]. A shift in the peak wavelength of a narrow band of transmitted or reflected wavelengths is observed with the change of a resonant coupling condition, caused by mechanical deformation of the structure [2,3,8]. Depending on device orientation and whether the substrate experiences tension or compression, the period of the structure either decreases or increases, resulting in a shift of the observed resonance from its original wavelength [4]. Thus, optical measurements of the wavelength change give indication of the mechanical deformation experienced by the PC. For such structures to serve as high resolution mechanical strain sensors, the bandwidth of the optical resonance should be as narrow as possible, so that small changes in the resonant optical wavelength can be easily discriminated. In addition, for PC-based strain sensors to find practical applications, they should be simple to fabricate, potentially over large surface areas so many transducers may be manufactured in parallel. The surface PC structures presented in this work function as narrowband reflectance filters with resonant peak widths of ~10 nm, enabling resonant wavelength shifts of <0.005 nm to be measured with a simple, robust detection instrument. Further, the surface PC structure is produced on the surface of silicone rubber or plastic using an accurate nanoreplica molding approach that is readily scaled to large surface areas, resulting in a device that is more easily fabricated than three-dimensional opal PC structures. Ultimately, such an approach may be scaled to attach large-area noncontact PC strain gauges to complex surfaces as a means for quantifying the strain distribution over surfaces exposed to various loading conditions.

Fig. 1 shows a detailed schematic diagram of the device concept used in this work. The sensor structure is a one-dimensional surface PC comprised of a low refractive index linear grating surface structure coated with a high refractive index film. For such a subwavelength structure, the 0th diffracted orders propagate while all higher orders are cut-off. Upon illumination with polarized white light at normal incidence, the evanescent ± 1st diffracted orders couple to counter-propagating leaky waves that form a standing wave within the periodically modulated layer [5]. Phase matching by the periodic structure to the reflected and transmitted 0th orders enables rapid extraction of energy from the leaky waves [4,9]. Constructive interference of the outcoupled light with the backward diffracted 0th order and destructive interference with the forward diffracted 0th order yields a sharp resonant reflection peak with 100% efficiency [10]. Therefore, when white light is incident onto the PC surface, light with wavelength λ is reflected with high efficiency, resulting in a peak in the collected wavelength spec-

* Corresponding author.
E-mail address: wpk@uiuc.edu (W.P. King).

0924-4247/$ – see front matter © 2010 Elsevier B.V. All rights reserved.
doi:10.1016/j.sna.2010.05.024

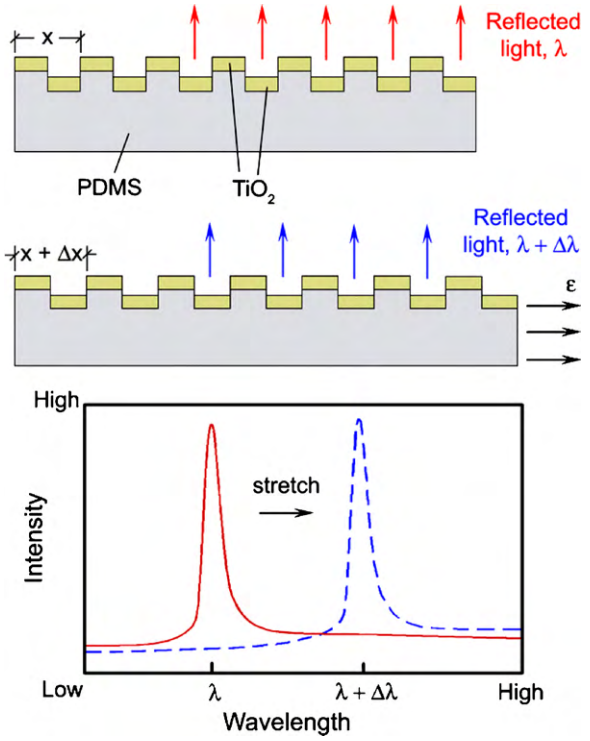

Fig. 1. Schematic of 1-D photonic crystal cross-section and wavelength shift under applied deformation.

trum. The resonant reflected spectrum coincides with a dip in the spectrum transmitted through the device.

For normal incidence illumination, the response of the PC is coupled to the 2nd order Bragg condition and therefore the spectral location of peak reflection, or peak wavelength value (PWV), can be given by:

$$\lambda = n_{\text{eff}}\Lambda \tag{1}$$

where λ is the resonant wavelength, n_{eff} is the effective index and Λ is the modulation period [5]. The effective index can be considered a weighted average of the refractive indices of the materials in which the standing wave generated at resonance, referred to as the "resonant mode", is supported. Assuming the materials comprising the PC have a constant refractive index, as a result of Eq. (1), the resonant reflected wavelength is linearly proportional to the PC period, resulting in peak shifts to longer wavelength when the sample is stretched.

Wavelength shift under induced strain has been observed in numerous materials, such as PC fibers [9], periodic composite films [3,4], and PCs, via simulations and experiments [11]. Deformation can be induced in a variety of ways, including mechanical [2,3], thermal, and electrostatic actuation [10] as well as through the use of piezoelectric material [12,13]. There have been only a small number of reports on strain measurement via stretching of a PC. Wong et al. [13] analytically examined wavelength shifts at strains of up to 0.2%, while Stomeo et al. [14] predicted 5.82 nm of wavelength shift for every GPa of applied unidirectional pressure. Ying et al. [15] demonstrated a wavelength shift of 212 nm under 20 kPa of applied stress in thin photonic band gap composite films, corresponding to more than 20% and 30% of tensile and compressive strains, respectively. The same trend was reported in synthesized plastic opal under applied pressure [2]. Pressure induced wavelength change was also observed by Arsenault et al. [11] during their demonstration of tunable PCs. In addition, strain measurements have been performed using PC fibers in a Sagnac interferometer configuration [9], with sensitivity and resolution of 0.23 pm/$\mu\varepsilon$ and 43 μm, respectively. However studies that report stretching based strain sensing of polymeric PCs [1,2] did not report resolution limits, which are required to understand how the technique could be implemented for sensing.

This paper describes experimental observations and complete characterization of a PC fabricated onto a highly elastic film used as a strain gage. Measurement stability, resolution limits, sensitivity, range, and linearity are reported in both qualitative and quantitative terms and compared to a traditional strain gage for reference purposes. Strain dependence on temperature is examined and quantified. The technique reported here has some advantages over previous reports of strain sensing with stretchable PCs because the current planar PC is much easier to fabricate than three-dimensional opal structures [1,2]. The sensitivity of the present structure is close to the sensitivity of the best sensitivity reported for photonic crystal strain gauges [2], while being much easier to manufacture.

2. Experiment

To address the challenges of small scale strain sensing, this paper describes experimental evidence of a wavelength shift of the light reflected from a continuously strained PC. Such an experiment is used to establish the relationship between applied strain and observed wavelength shift as well as to evaluate the most important parameters associated with strain gage application. Concurrent temperature monitoring accounts for and reduces the magnitude of measurement errors.

Conventional microfabrication processes were used to fabricate the device structure shown in Fig. 1 [8]. A poly(dimethylsiloxane) (PDMS) mixture was prepared by mixing Sylgard® 184 silicone elastomer base with a curing agent at a 10:1 ratio. After degassing, the mixture was poured over a silicon wafer mold that contains a linear grating surface structure (Λ = 550 nm, step height = 120 nm, 50% duty cycle) to form a ~2 mm thick layer. Curing was carried out at 140 °C for 20 min under low vacuum conditions. Once the PDMS layer was cured, it was peeled off the mold. Next, a 140 nm film of high refractive index (n = 2.0) TiO_2 was evaporated over the corrugated PDMS surface structure to form a 1-D PC with cross-section similar to that shown in Fig. 1. The sample was then cut to the desired size with length, the dimension perpendicular to the grating lines, kept as large as possible in order to achieve low strains under the condition of limited resolution of the current experimental setup.

After fabrication, device characterization was performed in the following manner. The PC grating structure was positioned between two grips that were separated by approximately 10 cm (L), one of which was stationary, while the other was allowed to translate vertically by means of an actuator. Such setup results in the direct translation of the induced stretch into strain values, ε, according to $\varepsilon = \Delta L/L$, where ΔL is the amount of stretch relative to the original grip positions. The PC may be positioned in a variety of orientations in the plane within which it is being stretched, relative to the direction of the grating lines, producing distinct optical spectra. For this experiment the grating lines were aligned horizontally to produce the largest possible wavelength shift during stretching. Optical resonances occur at distinct wavelengths for the structure of light with polarization oriented either parallel or perpendicular to the grating lines. The device was illuminated with light from a tungsten lamp through an optical fiber probe, which generates a resonant reflection at a wavelength of λ = 840.4 nm for light polarized parallel to the grating lines (TE mode) and a second resonant reflection at a wavelength of λ = 811.5 nm for light polarized perpendicular to the grating lines (TM mode) as shown in Fig. 2. The

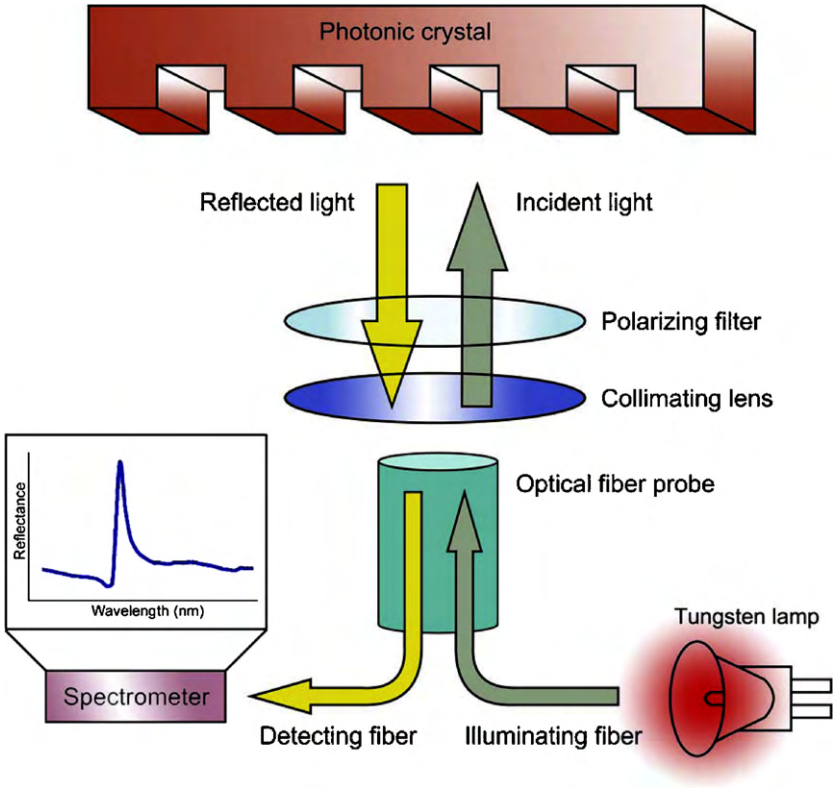

Fig. 2. Schematic of experimental setup. Photonic crystal is illuminated with light from tungsten lamp by means of the optical fiber; reflected light is collected by the detecting fiber and then sent to the spectrometer.

illuminated spot size is approximately 2 mm diameter. The TE mode has a resonant peak width at half maximum (FWHM) of 12.7 nm, while the TM mode has a resonant peak width of 8.4 nm. The TM mode was selected for monitoring changes in reflected wavelength due to applied stress, as the smaller linewidth allows greater precision. The appearance of the TE mode in the spectra collected by a second optical fiber that is bundled with the illumination fiber is suppressed by placing a linear polarizing filter in front of the illumination/collection probe head, with the polarizer oriented to illuminate and collect light with polarization perpendicular to the grating lines. The collection fiber was connected to the input port of a spectrometer (Ocean Optics USB2000). Software collected a single reflection spectrum every second by averaging 30 ms of data and determined the reflected peak wavelength value through an integrated fitting procedure. A traceable temperature meter was used for simultaneous temperature recording in the vicinity of the sample for low strain measurements as indicated in the next section.

3. Results and discussion

Fig. 3 shows typical atomic force microscope (AFM) images of the prepared sample. Before TiO_2 evaporation, the structure displays high uniformity with a period of ~550 nm, as indicated in Fig. 3(a). A cross-sectional view of the sample reveals that the grating lines have a sinusoidal cross-sectional profile, which is expected from the mold. The height of individual lines is changed slightly after dielectric deposition due to the high temperature at which this process is carried out as shown in Fig. 3(b). The period of the device remains close to that of the silicon master. However, some cracking is observed throughout the structure, which most likely develops because of the incompatibility of the stiffness and coefficient of thermal expansion in PDMS and TiO_2. The cracks are widely distributed, and did not interfere with the ability to measure resonant reflection peaks from the device surface. The TiO_2 thin film adhesion to PDMS was acceptable (no film peeling was observed after many expansion/relaxation experiments), although rigorous adhesion testing was not conducted. Due to the similarity of the grating step height and the deposited TiO_2 thickness, it is likely that the TiO_2 regions on the tops and bottoms of the grating teeth are not continuous, and that they become physically separated during stretching.

Upon recording a reflection spectrum for any given stretch of the PC, the shift in the wavelength of the main peak can be observed and quantified. Fig. 4 shows typical reflections at zero strain and 1% strain, which was 100 μm in this case. The shape of the collected spectrum is dictated by the optical properties of the PC under investigation. Two peaks are observed in each case, with the more intense one corresponding to the main reflection. The secondary peak arises from grating profile of the photonic crystal structure being slightly asymmetric with respect to the direction of light. As is apparent from the plot, when strain is applied, the peak shifts towards a higher wavelength. In addition, the reflection efficiency of the peak decreases with increased applied stretch due to the increased vertical separation of high refractive TiO_2 regions upon the upper and lower exposed horizontal surfaces of the structure as the stretch grows. This phenomenon results in overall reduction of the effective refractive index of the PC structure and gradual loss of the ability to sustain resonant modes, resulting in a limit in the range of possible strain measurement, and is consistent with previously published observations [1,3,4].

Reading stability over time is an important factor in strain measurement, as it is directly related to the repeatability and accuracy of results. Consistency is measured by collecting data at the same strain value for a prolonged period of time. Fig. 5 shows results of such an experiment with the sample held in an unstretched configuration. In an ideal case, the wavelength shift would be exactly zero over the entire time range. However, it fluctuated with

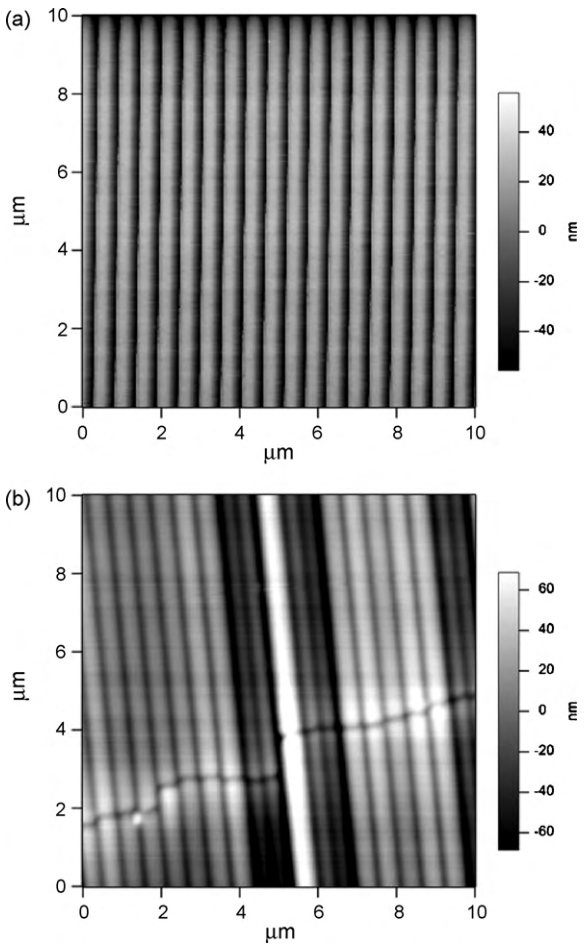

Fig. 3. AFM image of prepared photonic crystal sample: (a) before TiO_2 deposition; (b) after TiO_2 deposition; narrow crack runs through all grating lines.

0.1 nm maximum shift and 0.03 nm noise. Simultaneous temperature recording reveals that the PWV shift is inversely proportional to temperature as indicated with the dotted curve in Fig. 5. This behavior is observed due to the complex interaction between the displacements of each component in the system caused by thermal expansion or contraction, which in turn is induced through temperature variation. Based on recorded data, the wavelength shift can be adjusted for ambient conditions by establishing a correlation between temperature and the PWV. The correction factor is computed to be $\Delta\lambda = 0.11$ nm of wavelength shift toward lower wavelength per 1 °C temperature rise. The same type of correction is made for conventional foil strain gages to compensate for thermal output and gage material dependence on temperature.

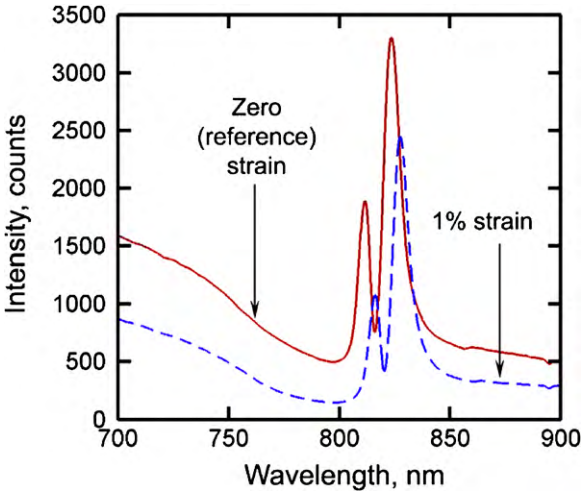

Fig. 4. Typical reflection spectrum for zero strain (red solid curve) and 1% strain (blue dashed curve). (For interpretation of the references to color in this figure legend, the reader is referred to the web version of the article.)

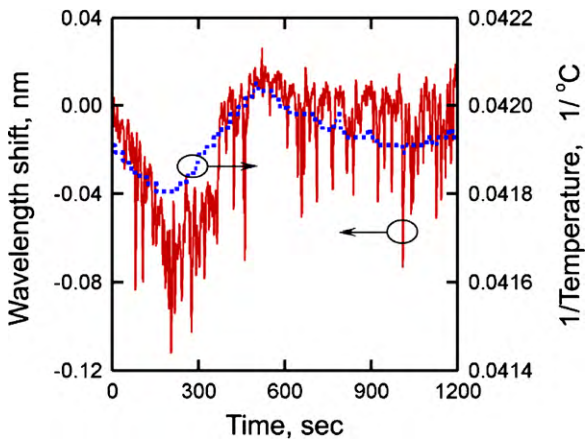

Fig. 5. Wavelength variation with temperature; red solid curve—wavelength shift with time, blue dotted curve—temperature variation with time.

In order to estimate the strain measurement resolution, the peak wavelength shift and its associated noise was determined for several strain ranges. This was done by varying the strain between zero and a chosen value every 3 min with the intent of establishing signal amplitude and repeatability in both wavelength shift and manual positioning. Fig. 6 shows data for 0–0.0078% strain steps. Because the micrometer-based translation stage has a measurement accuracy of 1 μm, the strain values reported have an accuracy of ±0.001 με%. Individual strain values are well separated, but exhibit significant variation in PWV shift even during 3 min intervals when deformation level is constant. Using the temperature-wavelength shift correlation discussed above paired with the temperature data collected during the experiment, the raw data was adjusted as indicated with circles in Fig. 6 by sub-

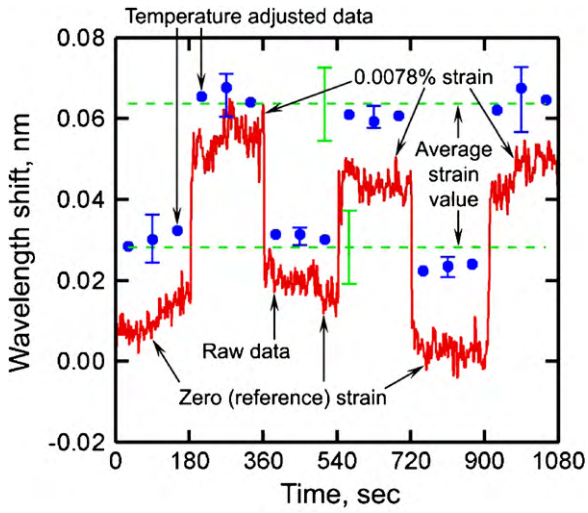

Fig. 6. Strain measurement resolution estimated at less than 0.0078% strain; red solid curve—collected data, blue points—data corrected for temperature variation, green dashed curve—average wavelength shift at specified strain; error bars represent three standard deviations from the respective mean. (For interpretation of the references to color in this figure legend, the reader is referred to the web version of the article.)

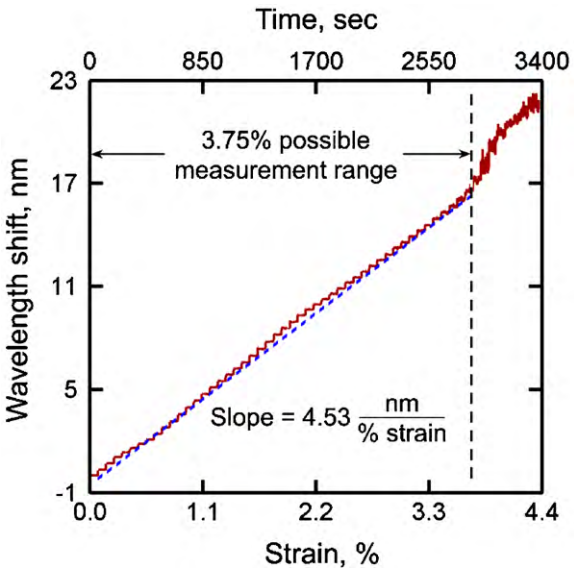

Fig. 7. Strain measurement range (red solid curve) and linearity (blue dotted curve); measurement can be carried out up to 3.75% strain; each step corresponds to 0.078% strain; linear fit is obtained by fitting strain data corrected for temperature variation up to 3.75%. (For interpretation of the references to color in this figure legend, the reader is referred to the web version of the article.)

tracting PWV shift due to temperature. Such correction results in less discrepancy and better consistency between the wavelengths of data points taken at the same strain value. Data averaging for each 1 min interval reduces the effect of random noise so that individual spikes are less pronounced. The observed wavelength differences between each group of averaged values are believed to be due to variations in the manual stretching and noise in the system, which also includes variation in ambient conditions other than temperature and setup vibration. The average value of the wavelength shift is shown with dashed lines with error bars indicating three standard deviations from the respective mean. The 0.015 nm gap between error bars means that smaller strain values could be detected. However, positioning accuracy of the current setup was limited to 10 μm, which corresponds to the 78 με strain given in Fig. 6. If the manual micrometer were to be replaced with a stage with high repeatability, the resolution of the measurement would be controlled solely by the noise, measured at 0.003 nm wavelength shift [16]. The noise-induced wavelength shift corresponds to 35 με. Although traditional strain gages are capable of detecting strains in sub-μm range, the resolution measured here is comparable to other measurements on PCs [14].

The resolution of a strain measurement is determined partially by the ability to mathematically determine the PWV by fitting the discrete set of wavelength points gathered by the spectrometer with a Lorentzian function [17]. This method of PWV determination enables interpolation between spectral data points, and subsequently higher wavelength resolution than provided by the spectrometer. The strain resolution will also be determined by the capability for the measured structure to remain in a fixed state between subsequent measurements, where physical processes such as mechanical vibration of the sample/probe and thermal stability will provide limits to detection resolution.

The sample was subjected to 0.078% strain steps in 1 min intervals as seen in Fig. 7. Steps were necessary in order to allow the sample to stabilize at a particular strain value and to filter out random fluctuations by averaging the specified number of data points recorded during each step. PWV values were corrected for temperature variation for more accurate results using the procedure outlined above and depicted in Fig. 5. The sample was stretched

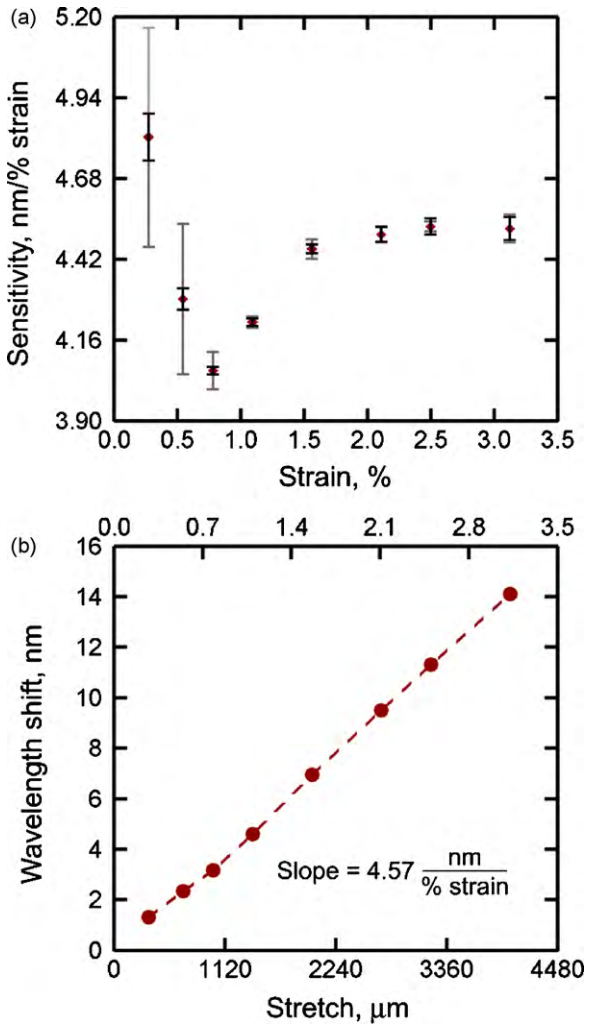

Fig. 8. (a) Measurement sensitivity and repeatability at several strain values; gray error bars—uncertainty in repeatability, black error bars—uncertainty due to noise in the system; error bars represent three standard deviations from the mean; (b) linear response obtained from sensitivity data.

to 4.4% total strain, although the graph indicates that reliable measurements can only be carried out up to 3.75% strain. This is well within the range of general purpose strain gages, which are generally capable of measuring 3–5% strain. Measurement noise increases with increasing stretch due to the reduced intensity of the peak at higher strain values, also noted in Fig. 4. Lower peak height translates into greater width at half maximum, which in turn means that measurement resolution is decreased.

Fig. 7 shows a curve fit to strain measurements between 0% and 3.75% strain. The curve is obtained by adjusting the raw data for temperature variation, averaging data within 1 min intervals, and then fitting a straight line to the averages. The result is highly linear over the entire range with the sensitivity of approximately 4.5 nm of wavelength shift per percent strain. This sensitivity is close to the best sensitivity reported for photonic crystal strain gauges [1,2]. Slight deviation from linearity is again due to manual positioning error and system noise.

Fig. 8 shows that the present measurement exhibits improvement in linearity following a slight initial stretch. Error in manual positioning dominates repeatability behavior at low strains, causing large variations in sensitivity at these values as indicated with gray error bars in Fig. 8(a). Since the magnitude of positioning error is constant over the entire strain range, the observed sensitivity error decreases with increased deformation because positioning

uncertainty constitutes smaller percentage of the entire stretch at higher strains. This also causes the initial sensitivity oscillations to be damped out at higher strains, where the measurement becomes highly repeatable. On the other hand, at larger induced deformations, sensitivity is limited by noise, shown with black error bars. Uncertainty due to noise in the system is smaller than the initial positioning uncertainty. As can be seen from the black error bars in Fig. 8(a), the amount of noise decreases initially, reaches its smallest value around 0.85% strain, and then increases until maximum possible deformation is reached. Noise fluctuation with stretch is observed due to the intensity variation of the fitted peak, similar to that shown in Fig. 4. In order to increase overall measurement range, the initial stretch is chosen such that the peak height at zero strain is below its possible maximum. The solid curve of Fig. 4 corresponds to this case. Owning to the relative nature of strain measurements, the initial wavelength spectrum can be taken at any convenient sample stretch. The peak intensity first increases, resulting in diminishing noise level, and then becomes smaller (dashed curve, Fig. 4) until it disappears almost completely. This occurs at 3.75% strain, shown in Fig. 7.

Fig. 8(b) further confirms measurement repeatability and sensitivity characterized by the slope of the response curve when it is given as a function of mechanical deformation. The points in Fig. 8(b) are obtained from sensitivity data by averaging the wavelength shift values from six experimental runs. The response is similar to that in Fig. 7 with the two slopes being equal within experimental error. The standard deviation for all points is less than 0.05 nm, corresponding to the noise in the data as was described above.

Optical strain measurement has several advantages over traditional foil strain gages. Soldering of electrical connections, current heating effects and noise due to electric and magnetic fields as well as tedious installation procedures for the gage itself are eliminated, although this technique still suffers from temperature dependency and transverse sensitivity. Also, compared to most metals whose strain is to be measured, PDMS has very low Young's modulus and large elongation range. Thus, stretchable strain gages are good candidates for strain measurement on nonstiff materials.

It is reasonable to expect that the technique described here could be modified to measure significantly smaller strains than those demonstrated here. The main limit to our approach is the mechanical fixture, which would be much different in any practical strain sensing application. Other noise sources accounted for a resolution limit of 35 $\mu\varepsilon$, which may or may not be improved through enhanced optics and improved temperature compensation. Given a detection limit of 78 $\mu\varepsilon$, considerable improvement could be offered by employing optics that can probe substantially smaller regions of the photonic crystal surface. It is reasonable to expect that the optical signal into the spectrometer could be collected from a spot on the PC of 10 μm or smaller using a detection instrument for measuring resonant wavelength shifts similar to that shown in [5]. Detection of 78 $\mu\varepsilon$ within a 10 μm spot yields detection of sub-nm lateral deformation. Both the 10 μm lateral resolution and the sub-nm strain sensing are considerable improvements beyond what is possible with conventional mechanical strain gauges.

4. Conclusion

This paper reports experimental evaluation of a stretched PC for use as a strain gage, by measuring the wavelength shift as a function of applied stretch. The device resolution is much less than 78 $\mu\varepsilon$, currently limited by the resolution of a manual micrometer, while sensitivity is 4.53 nm of wavelength shift per 1% of applied strain. The sensitivity is comparable to the best results in the literature while being easy to fabricate. The measurement was highly linear and its range was 3.75% strain, comparable to that of a conventional strain gages. The measurement had a strong temperature dependence, which could be compensated for improved measurements. This measurement method is an alternative to standard strain measurement and may prove to be useful for situations where wiring is not possible or where the low spring constant of the strain gauge material benefits the measurement. While the sensor surface must be optically accessible to a normal-incidence optical fiber probe, we anticipate that this measurement approach would be compatible with low cost packaging methods, as the sensor itself does not require a source of power. We envision that a single illumination source would be able to supply light to a distributed array of sensors, connected by optical fiber, and that a single miniature spectrometer could serve to rapidly monitor the sensor array. With appropriate improvements in the optical signal collection, the approach could be improved to sub-nm resolution.

References

[1] J. Li, Y. Wu, J. Fu, Y. Cong, J. Peng, Y. Han, Reversibly strain-tunable elastomeric photonic crystals, Chemical Physics Letters 390 (May 2004) 285–289.
[2] K. Yoshino, Y. Kawagishi, M. Ozaki, A. Kose, Mechanical tuning of the optical properties of plastic opal as a photonic crystal, Japanese Journal of Applied Physics 38 (July 1999) 786–788.
[3] J.M. Jethmalani, W.T. Ford, Diffraction of visible light by ordered monodisperse silica-poly(methyl acrylate) composite films, Chemistry of Materials 8 (1996) 2138–2146.
[4] S.H. Foulger, P. Jiang, A.C. Lattam Jr., D.W. Smith, J. Ballato, Mechanochromic response of poly(ethyleneglycol) methacrylate hydrogel encapsulated crystalline colloidal arrays, Langmuir 17 (2001) 6023–6026.
[5] W. Suh, M.F. Yanik, O. Solgaard, S. Fan, Photonic crystal reflectors/filters and displacement sensing applications, US Patent 7,155,087 (December 2006).
[6] M. Boroditsky, R. Vrijen, T.F. Krauss, R. Coccioli, R. Bhat, E. Yablonovitch, Spontaneous emission extraction and purcell enhancement from thin-film 2-D photonic crystals, Journal of Lightwave Technology 17 (1999) 2096–2112.
[7] M. Boroditsky, T.F. Krauss, R. Coccioli, R. Vrijen, R. Bhat, E. Yablonovitch, Light extraction from optically pumped light-emitting diode by thin-slab photonic crystals, Applied Physics Letters 75 (1999) 1036–1038.
[8] N. Ganesh, I.D. Block, B.T. Cunningham, Near UV-wavelength photonic crystal biosensor with enhanced surface-to-bulk sensitivity ratio, Applied Physics Letters 89 (2006) 023901–023904.
[9] X. Dong, H.Y. Tam, P. Shum, Temperature-insensitive strain sensor with polarization-maintaining photonic crystal fiber based Sagnac interferometer, Applied Physics Letters 90 (April 2007) 1–3.
[10] D.E. Sene, V.M. Bright, J.H. Comtois, J.W. Grantham, Polysilicon micromechanical gratings for optical modulation, Sensors and Actuators A 57 (1996) 145–151.
[11] A.C. Arsenault, T.J. Clark, G. von Freymann, L. Cademartiri, R. Sapienza, J. Bertolotti, E. Vekris, S. Wong, V. Kitaev, I. Manners, R.Z. Wang, S. John, D. Wiersma, G.A. Ozin, From colour fingerprinting to the control of photoluminescence in elastic photonic crystals, Nature Materials 5 (2006).
[12] G.F. Williams, Optical path length modulator, US Patent 5,313,535 (May 1994).
[13] C.W. Wong, X. Yang, P.T. Rakich, S.G. Johnson, M. Qi, Y. Jeon, G. Barbastathis, S.-G. Kim, Strain-tunable photonic bandgap microcavity waveguides in silicon at 1.55 μm, Proceedings of SPIE—the International Society for Optical Engineering 5511 (2004) 156–164.
[14] T. Stomeo, M. Grande, A. Qualtieri, A. Passaseo, A. Salhi, M. De Vittorio, D. Biallo, A D'Orazio, M. De Sario, V. Marrocco, V. Petruzzelli, F. Prudenzano, Fabrication of force sensors based on two-dimensional photonic crystal technology, Microelectronic Engineering 84 (May/August 2007) 1450–1453.
[15] Y. Ying, J. Xia, S.H. Foulger, Pressure tuning the optical transmission properties of photonic band gap composites, Applied Physics Letters 90 (2007).
[16] B.T. Cunningham, P. Li, B. Lin, J. Pepper, Colorimetric resonant reflection as a direct biochemical assay technique, Sensors and Actuators B 81 (2002) 316–328.
[17] P. Li, B. Lin, J. Gerstenmaier, B.T. Cunningham, A new method for label-free imaging of biomolecular interactions, Sensors and Actuators B 99 (2004) 6–13.